STUDY ON BORON EMITTER FORMATION BY BBR_3 DIFFUSION FOR N-TYPE SI SOLAR CELL APPLICATIONS

Yvonne Schiele, Simon Fahr, Sebastian Joos, Giso Hahn, Barbara Terheiden
University of Konstanz, Department of Physics, P.O. Box 676, D-78457 Konstanz, Germany
Phone: +49 (0) 7531 88 4995, Fax: +49 (0) 7531 88 3895, Email: Yvonne.Schiele@uni-konstanz.de

ABSTRACT: Solar cells based on n-type c-Si wafers have raised growing interest since they feature clear advantages compared to the standard p-type Si substrates. A promising technology to establish the n-type solar cell's p-n junction is thermal diffusion of boron atoms into the Si surface from a boron tribromide (BBr_3) source. Boron emitters are characterized in terms of surface doping density, depth and shape of the doping profile, resulting sheet resistance and its uniformity on a large-area wafer as well as emitter saturation current density. In addition, the emitter is to be utilizable in a solar cell production process aiming at an undiminished carrier lifetime in the Si substrate, a reduction of process duration and good removability of the borosilicate glass layer. By optimizing these emitter characteristics, the efficiency of n-type solar cells can be significantly enhanced. In order to achieve a desired boron emitter, diffusion process parameters such as temperatures, gas flows and periods of individual process steps are systematically varied. Predictions which kinds of emitters will result from various process parameters can be derived, helping to understand the B emitter formation from a BBr_3 source.
Keywords: n-type, Boron, Diffusion

1 INTRODUCTION

Solar cells based on n-type doped crystalline silicon wafers have raised growing interest in the recent past (e.g. [1-4]) since they feature obvious advantages compared to the standard p-type Si substrate material: n-type solar cells can generally attain higher conversion efficiencies since minority carrier lifetimes are less affected by certain impurities [5] and their efficiency does not suffer from the boron-oxygen complex related light induced degradation [6].

There are several n-type solar cell concepts with various mechanisms for establishing the p-n junction. For instance, applying the industrial standard processing sequence for p-type Si solar cells to n-type substrates, known as the PhosTop concept, has proven a simple and economical fabrication method for n-type Si solar cells featuring an aluminum alloyed emitter at the rear of the solar cell (e.g. [7-9]). In heterojunction solar cells, the emitter consists of an amorphous material (e.g. a-Si) which at the same time provides surface passivation [10]. This high efficiency solar cell concept approach can be implemented without any masking steps at temperatures below 200°C [11].

A frequently employed alternative to establish the p-n junction of an n-type solar cell is the incorporation of boron atoms into the silicon wafer. On the one hand, this can be implemented by depositing (e.g. PECVD or APCVD) boron doped a-SiO_x and subsequently exposing it to high temperatures (e.g. [12-14]). On the other hand, boron can be incorporated by ion implantation followed by high-temperature annealing (e.g. [15-17]). A further promising technology is direct thermal diffusion of boron from a boron trichloride (BCl_3) (e.g. [18]) or boron tribromide (BBr_3) source.

In the BBr_3 diffusion process, nitrogen is bubbled through liquid BBr_3, and conducted into the diffusion tube together with oxygen. There, boron is dissociated from the BBr_3 molecule and forms a boron trioxide (B_2O_3) layer on the silicon wafer surface (Eq. 1). At the interface, the B_2O_3 reacts with the Si to silicon dioxide releasing elementary boron which can then diffuse into the silicon bulk (Eq. 2).

$$4BBr_3 + 3O_2 \rightarrow 2B_2O_3 + 6Br_2 \quad (1)$$

$$2B_2O_3 + 3Si \rightarrow 4B + 3SiO_2 \quad (2)$$

The SiO_2/B_2O_3 stack is also known as borosilicate glass (BSG) which has to be removed after the diffusion step in a solar cell production process. The BBr_3 diffusion takes place at temperatures above 900°C to allow the working of both the interstitial and vacancy diffusion mechanism of boron [19].

Boron doping profiles resulting from BBr_3 diffusions typically exhibit a concentration decline towards the wafer surface, the so-called pile-down. This is due to a higher solubility of B in SiO_2, grown during diffusion, than in Si.

Simulations can determine the optimal boron emitter to be utilized in a particular n-type c-Si solar cell. Properties of such an emitter are, for instance, the doping atom concentration at the surface $[B]_{surf}$, depth and shape of the doping profile, resulting sheet resistance R_{sh} and its uniformity on a large-area wafer as well as emitter saturation current density j_{0e} depending on the passivation layer. In general, a higher doping concentration allows lower contact resistivity but also leads to higher saturation current densities as it is the case for deeper profiles, too. However, emitters with too flat profiles are at risk to be shunted by fired-through metal contacts.

The boron emitter properties can be modified by varying parameters of the BBr_3 diffusion process such as temperatures, gas flows and durations of individual process steps. Optimizing the emitter regarding the afore mentioned characteristics can finally enhance the efficiency of n-type Si solar cells significantly.

In addition, we attach importance to the capability of the designed emitter to be utilized in an industrial solar cell production process. The predominant aims in this respect are reduction of boron emitter diffusion period and good removability of the BSG layer emerged on the wafer surface.

2 EXPERIMENTAL

2.1 Organization of the study

In order to achieve the desired properties of the boron emitter, processing parameters of the BBr_3 diffusion (temperature, BBr_3 flow, flow of nitrogen as carrier gas and deposition period) are systematically varied and the resulting boron emitters are characterized in terms of the designated properties. Furthermore, minority carrier lifetime τ_{eff} of the Si substrate is determined to examine the causing of defects and/or contamination by impurities during high temperature diffusion. Based on emerging trends, predictions which kind of emitter will result from given process parameters can be derived, helping to understand the specific processes occurring during B emitter formation from a BBr_3 source. For the optimization of BSG removability, BSG layer thickness is determined and correlated with the corresponding color. A possible connection of thickness with resistance distribution on the wafer area is investigated.

2.2 Sample preparation and characterization techniques

All samples are subjected to a standard RCA cleaning [20] prior to BBr_3 diffusion. Afterwards, the BSG layer is removed in diluted HF (concentration starting at 2%, successively raised up to 10% if not sufficient for removal) allowing the detailed emitter characterization.

For the investigation of surface doping concentration and emitter depth profile, large-area (156×156 mm^2) n-type Czochralski (Cz) Si wafers (2-5 Ωcm) are utilized as base material and the emitter is measured by electrochemical capacitance voltage (ECV) profiling. To examine the content of electrically inactive boron atoms, secondary ion mass spectrometry (SIMS) is complementarily carried out. The same wafers are also employed for R_{sh} mapping by four-point probe (4PP) technique at 5×5 measurement points distributed on the wafer area and by a spatially resolved capacitive photodiode potential difference method using a Semilab WT2000 tool.

The R_{sh} data from 4PP measurement are illustrated as boxplots in order to compare the R_{sh} uniformity on a large-area wafer. The box corresponds to the data range where the middle 50% of data are located, bordered by the upper and lower quartile and sectioned by the median, whereas the arithmetic mean is represented by the horizontal line (mostly inside the box). The length of the vertical “antennae” outside the box indicates those values deviating from the upper/lower quartile by maximally one and a half times the interquartile distance. Maximum and minimum values are depicted as a cross. Supplementarily, the measured values themselves are shown beside.

The j_{0e} samples (50×50 mm^2, 250 µm thick) consist of high-ohmic (5-10 Ωcm) chemically polished n-type float-zone (FZ) Si base material. The emitter is passivated by 30 nm Al_2O_3 (atomic layer deposited, ALD) on both sides using a FlexAL device from Oxford Instruments followed by an annealing step in nitrogen atmosphere at 420°C to activate the passivation. By means of a Sinton Lifetime Tester, j_{0e} is determined from photoconductance decay measurement which is evaluated at an injection level of $\Delta n = 1\times10^{16}$ cm^{-3} (high level injection mode) [21]:

$$\frac{1}{\tau_{\text{eff}}} - \frac{1}{\tau_{\text{Auger}}} = \frac{1}{\tau_{\text{SRH}}} + \frac{2j_{0\text{e}}}{q n_{\text{i}}^2 W}\Delta n \qquad (3)$$

with Auger and Shockley-Read-Hall carrier lifetime τ_{Auger} and τ_{SRH}, q being the elementary charge, $n_i = 8.6\times10^9$ cm^{-3} the intrinsic carrier concentration and W the wafer thickness. For τ_{Auger}, the parameterization of Kerr et al. [22] is applied.

For the minority carrier lifetime samples, 1 Ωcm n-type FZ Si wafers (50×50 mm^2, 500 µm thick) are used. After diffusion, the emitter is removed in a chemical polishing solution (10 µm Si removal per side) followed by cleaning in a piranha solution with subsequent HF dip. Afterwards, the wafers are passivated by a quinhydrone methanol (QM) solution and τ_{eff} is determined by the photoconductance decay method at $\Delta n = 1\times10^{15}$ cm^{-3}.

After BBr_3 diffusion, the color distribution of the BSG layer is photographically mapped. In order to measure the thickness of the BSG layer, mechanically polished FZ Si wafers are utilized. On several sites on the wafer exhibiting different BSG colors, the BSG is partially coated by a photolithography mask, followed by removing the BSG in the non-capped area in an HF solution. Subsequently, the mask is removed but with BSG remaining beneath. Via atomic force microscopy (AFM), BSG thickness is then determined at the created stair.

3 RESULTS

3.1 BBr_3 diffusion process

The BBr_3 diffusion process is subdivided into four main steps. After being started by a heating-up to diffusion temperature and a stabilizing phase (A), it is continued by the actual BBr_3 deposition (B), followed by a drive-in step (C), and is finished by cooling-down (D). During step (A) and (C), N_2 and O_2 flow through the tube yielding a thin oxide layer on the wafer surface prior to BBr_3 deposition (B). During phase (B), BBr_3 is conducted into the diffusion tube (via N_2 flow through the bubbler) in addition to an N_2 carrier gas and O_2 flow. Solely N_2 flows during the last step (D).

Each of the subsequent percentages corresponds to a certain absolute value of the investigated and varied parameters. The basis of the percentages should be noticed to have been chosen arbitrarily and the percentages themselves apply only to a relative comparison.

3.2 BBr_3 flow during deposition

Varying the BBr_3 flow during the deposition step (B) over a large range does not lead to a significant change in sheet resistance (Fig. 1&2). A BBr_3 flow of less than 25%, however, does not dope the wafer sufficiently anymore.

Irrespective of this very low BBr_3 flow, the doping profiles do not differ significantly over a wide range of depth for the relevant boron concentration magnitudes. Below $[B] \approx 10^{19}$ cm^{-3}, the variations exhibit no evident trend and are interpreted to be measuring uncertainties as only few ECV measurement points represent this low doping density range.

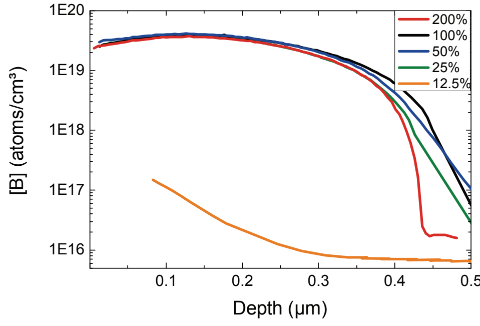

Figure 1: Depth profile of boron concentration measured by ECV profiling for different BBr_3 flows. Remaining parameters: N_2 flow = 100%, dep. period = 100%, Ref. temperature.

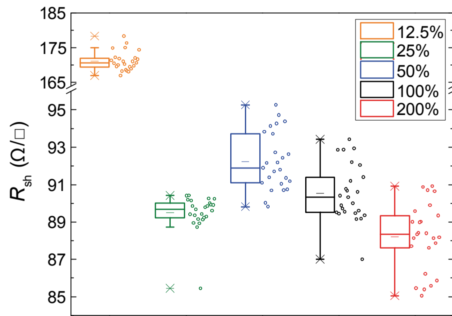

Figure 2: R_{sh} distribution on a 156×156 mm^2 wafer measured by 4PP method for different BBr_3 flows. Remaining parameters as specified in Fig. 1.

Therefore, at a BBr_3 flow of ≥25%, the doping source can be considered infinite, thus the boron content in the BSG layer formed on the wafer surface is not the limiting factor regarding the amount of boron diffusing into the wafer. By increasing this flow, doping concentration cannot be further raised.

The highest degree of uniformity for a reasonable R_{sh} is obtained at 25% BBr_3 flow (Fig. 2). The considerably more uniform R_{sh} distribution of the 25% BBr_3 flow diffusion compared to the ones with higher BBr_3 flows is illustrated by a spatially resolved R_{sh} measurement (Fig. 3).

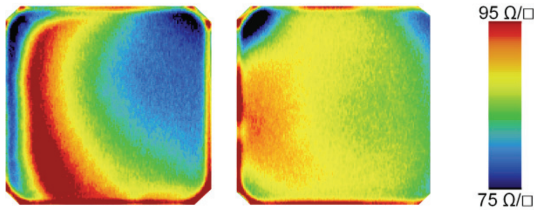

Figure 3: R_{sh} distribution on a 156×156 mm^2 wafer determined with a Semilab WT2000 tool after diffusion with 100% and 25% (right) BBr_3 flow. Remaining parameters as specified in Fig. 1.

Also, the BSG color distribution resulting from diffusions with high BBr_3 flow is significantly less uniform than the one from lower BBr_3 flow diffusions (Fig. 4). AFM measurements reveal that this color variation can be correlated with BSG layer thickness. BSG thickness varies from 10 nm (transparent) to 150 nm (light blue) and even more.

Hence, for BBr_3 flows up to 25%, the BSG layer grows in uniform thickness. However, BBr_3 flows ≥50% yield BSG layers with partially greater thickness, thus diminishing thickness uniformity and correspondingly increasing R_{sh} nonuniformity. Up to a certain thickness, the BSG layer seems to grow uniformly because the reactions (1) & (2) may be controlled by the reaction activity of their reactants. During this growth, the SiO_2 interface layer thickness is continuously increasing. From a certain SiO_2 thickness on, the reactions (1) & (2) seem to be increasingly influenced by local differences on the wafer, like e.g. gas flow or temperature, which may also yield a nonuniform emitter.

Removal of BSG in HF is easier the thinner the layer thickness. In areas with very thick layers (~150 nm), the BSG remains on the wafer surface even with high HF concentrations up to 10% and etching durations up to 45 min, whereas BSG layers with typical thicknesses for 25% BBr_3 flow are already removable in 5% HF.

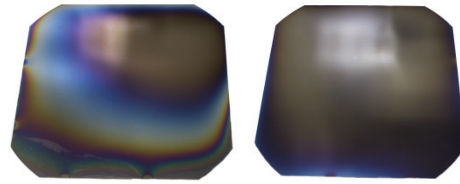

Figure 4: BSG distribution on a 156×156 mm^2 wafer after diffusion with 200% (left) and 50% (right) BBr_3 flow. Remaining parameters as specified in Fig. 1.

Minority carrier bulk lifetime in the silicon substrate continuously diminishes with rising BBr_3 flow (Tab. I). Hence, the BBr_3 itself, products of the chemical reactions with BBr_3 or electrically inactive boron atoms cause defects and/or contamination by impurities in the silicon substrate during high temperature diffusion. Defects may also originate from strains occurring especially with thick BSG layers. For a low BBr_3 flow of 12.5%, however, τ_{eff} reduction is small enough not to significantly impair solar cell efficiency.

Table I: Effective minority carrier lifetime in the Si substrate after BBr_3 diffusion for different BBr_3 flows and without prior BBr_3 diffusion (0%). Remaining parameters as specified in Fig. 1.

BBr_3 flow (%)	τ_{eff} (µs)
0	1200
12.5	900
200	400

3.3 N_2 carrier gas flow during deposition

Varying the N_2 carrier gas flow during BBr_3 deposition (B), no difference in R_{sh} is observable for 50% and 100% (Fig. 5). Also, the doping profiles measured by ECV do not differ considerably (not depicted). However, for 200% gas flow, the boron content in the diffusion tube is too much diluted to attain a reasonable doping.

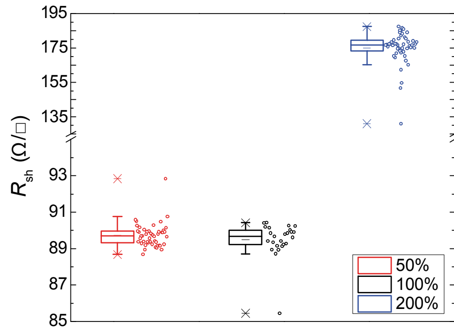

Figure 5: R_{sh} distribution on a 156×156 mm^2 wafer measured by 4PP method for different N_2 carrier gas flows. Remaining parameters: BBr_3 flow = 25%, dep. period = 100%, Ref. temperature.

3.4 Deposition period

The longer the BBr_3 deposition period the deeper are the boron atoms driven into the Si substrate (Fig. 6). The depth of maximal doping concentration, however, remains almost constant. Moreover, for elevated deposition periods (300%), doping concentration over the whole emitter depth increases and the pile-down effect can be reduced slightly. These observations, however, heavily depend on the position on the wafer where the profile is determined (see Fig 7).

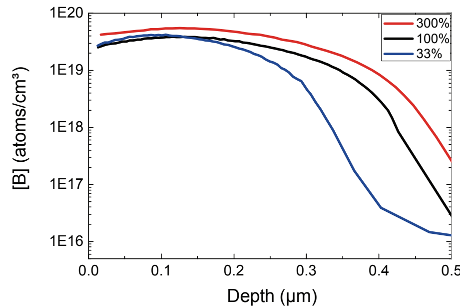

Figure 6: Depth profile of boron concentration measured by ECV profiling for different BBr_3 deposition periods. Remaining parameters: BBr_3 flow = 25%, N_2 flow = 100%, Ref. temperature.

According to the 4PP measurements, a tripled BBr_3 deposition period only causes a broader spreading of sheet resistance values on a large-area wafer, whereas a shortening to one third increases R_{sh} by 15% (Fig. 7).

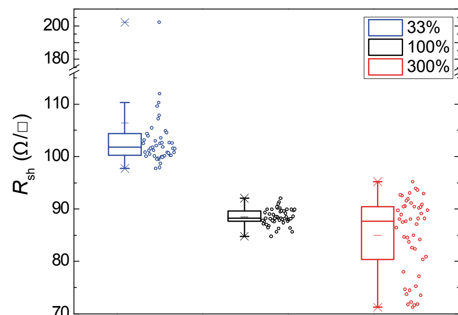

Figure 7: R_{sh} distribution on a 156×156 mm^2 wafer measured by 4PP method for different BBr_3 deposition periods. Remaining parameters as specified in Fig. 6.

Thus, up to a deposition period of 100%, the thickness of our BSG is uniform. For a 300% deposition period, however, this BSG becomes thicker, but only in some areas of the wafer, inducing a nonuniform sheet resistance. This effect is similar to the thicker but nonuniform BSG layer caused by higher BBr_3 flows (see 3.2). Accordingly, from a certain thickness on, our BSG seems to grow nonuniformly in general.

Saturation current density decreases with deposition period (Tab. II), corresponding to the R_{sh} variation and distribution on the wafer area and therefore to the overall amount of boron within the emitter.

Besides, a longer deposition period is not preferable as it extends the overall process duration.

Table II: Emitter saturation current density, corresponding sheet resistance (median from 4PP measurement) and profile depth (defined as depth with 1% of $[B]_{surf}$) for different BBr_3 deposition periods. Remaining parameters as specified in Fig. 6.

BBr_3 deposition period	33%	100%	300%
j_{0e} (fA/cm^2)	11	22	33
R_{sh} (Ω/)	102	88	87
Profile depth (µm)	0.36	0.45	0.49

3.5 Process temperature

A temperature variation by only 20 K already has a major influence on R_{sh} due to an enhanced diffusion of boron into silicon with higher temperatures (Fig. 8&9). Whereas boron concentration at the surface is not modified significantly, the profile is driven in deeper with higher diffusion temperature (Fig. 8).

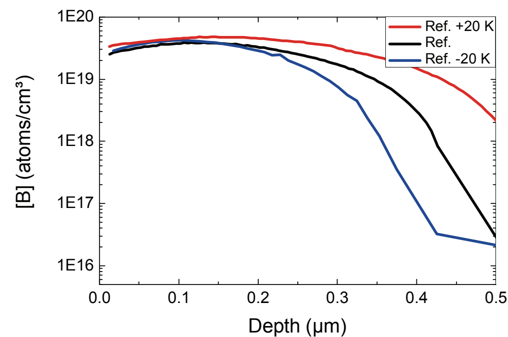

Figure 8: Depth profile of boron concentration measured by ECV profiling for different diffusion temperatures. Remaining parameters: BBr_3 flow = 25%, N_2 flow = 100%, dep. period = 100%.

A temperature reduction by 20 K leads to an R_{sh} increase of 25% and a broader distribution, whereas a higher temperature (+20 K) causes analogously lower R_{sh} values (Fig. 9).

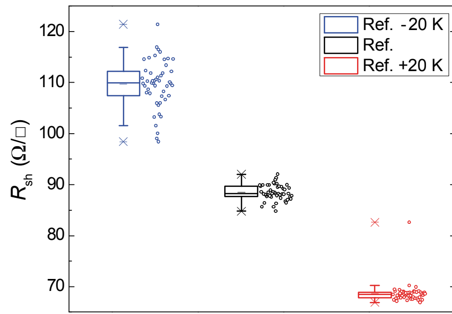

Figure 9: R_{sh} distribution on a 156×156 mm^2 wafer measured by 4PP method for different diffusion temperatures. Remaining parameters as specified in Fig. 8.

3.6 Content of electrically active doping atoms

A comparison of a boron doping profile measured by ECV with the corresponding SIMS profile reveals the amount of boron atoms not contributing to the electrical conductivity of the emitter as being negligible (Fig. 10).

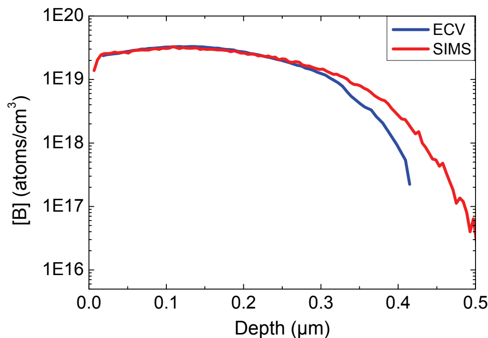

Figure 10: Depth profile of the identical boron emitter measured by ECV profiling and by SIMS (diffusion parameters: BBr_3 flow = 25%, N_2 flow = 100%, dep. period = 100%, Ref. temperature).

4 CONCLUSION & OUTLOOK

Characterizing the boron emitters generated by BBr_3 diffusion carried out at systematically varied process parameters, initial results and trends can be stated.

Varying the BBr_3 flow during the deposition step over a wide range does not lead to a significant change in R_{sh}. The doping source can be considered infinite, thus the B content in the BSG layer is not the limiting factor regarding the amount of B diffusing into the wafer. Increasing this flow does not yield a higher doping concentration. Maximal R_{sh} uniformity is obtained at very low BBr_3 flows. AFM measurements reveal that the BSG color variation correlates with BSG layer thickness. Thus, higher BBr_3 flows generate BSG layers with diminishing thickness uniformity and thus increasing R_{sh} nonuniformity as well. BSG layers with typical thicknesses for low BBr_3 flows are easily removable in 5% HF. τ_{eff} in the substrate continuously diminishes with increasing BBr_3 flow. Hence, the BBr_3 itself or products of the chemical reactions with BBr_3 cause defects and/or contamination by impurities in the silicon substrate during high temperature diffusion.

A shortening to one third of BBr_3 deposition period raises R_{sh} by 15%, whereas a tripled period causes only a broader spreading of the R_{sh} values on a large-area wafer. Thus, for very high deposition periods, BSG becomes thicker, but only in some areas of the wafer, inducing a nonuniform sheet resistance, similarly to the thicker but nonuniform BSG layer caused by higher BBr_3 flows. Corresponding to the R_{sh} variation and distribution on the wafer area and therefore the overall amount of boron within the emitter, j_{0e} decreases with deposition period.

A 20 K diffusion temperature increase reduces R_{sh} by 20 Ω/□ due to an enhanced diffusion of boron into silicon. Whereas boron concentration at the surface is not modified significantly, the profile is driven in deeper.

Virtually all boron atoms in the emitter contribute to its electrical conductivity for the investigated parameters.

By systematic variation of the process parameters, a uniform high efficiency boron emitter with an R_{sh} of approximately 100 Ω/□ and a j_{0e} of 20 fA/cm^2 has been created whose BBr_3 diffusion does not reduce carrier lifetime in the Si bulk to an extent which significantly limits solar cell efficiency. The first manufactured solar cells featuring this emitter yield promising results [23] with specific contact resistivities of ~4 mΩcm^2 if screen-printed AgAl pastes are used.

Further process variations need to be conducted to elaborate the emerging trends which permit to predict the resulting emitters based on given process parameters and to more profoundly understand the specific processes occurring during B emitter formation from a BBr_3 source. Finally, the boron emitter yielding maximal solar cell efficiency according to simulations can be implemented into solar cell processing.

5 ACKNOWLEDGEMENTS

The authors would like to thank L. Mahlstaedt and S. Riegel for fruitful discussions and processing assistance. The research leading to these results has received funding from the European Union Seventh Framework Programme (FP7/2007-2013) for the Collaborative Project (CP) '20plµs' with the full title: 'Further development of very thin wafer based c-Si photovoltaics' under grant agreement n° 256695. The content of this publication is the responsibility of the authors.

6 REFERENCES

[1] J. Zhao, A. Wang, P.P. Altermatt, M.A. Green, J.P. Rakotoniaina, O. Breitenstein, Proc. 29th IEEE PVSC, New Orleans, USA (2002) 218.
[2] F. Kiefer, C. Ulzhöfer, T. Brendemühl, N.-P. Harder, R. Brendel, V. Mertens, S. Bordihn, C. Peters, J.W. Müller, IEEE J. Photov. 1 (1) (2011) 49.
[3] J. Benick, B. Hoex, M.C.M van de Sanden, W.M.M. Kessels, O. Schultz, S.W. Glunz, Appl. Phys. Lett. 92 (2008) 253504.
[4] F. Book, T. Wiedenmann, G. Schubert, H. Plagwitz, G. Hahn, En. Proc. 8 (2011) 487.
[5] D. Macdonald, L.J. Geerligs, Appl. Phys. Lett. 85 (2004) 4061.
[6] S.W. Glunz, S. Rein, J.Y. Lee, W. Warta, J. Appl. Phys. 90 (2001) 2397.
[7] D.L. Meier, H.P. Davis, R.A. Garcia, J. Salami, A. Rohatgi, A. Ebong, P. Doshi, Sol. En. Mat. & Solar Cells 65 (2001) 621.

[8] Y. Schiele, F. Book, S. Seren, G. Hahn, B. Terheiden, En. Proc. 27 (2012) 460.
[9] Y. Schiele, S. Wilking, F. Book, T. Wiedenmann, G. Hahn, En. Proc. 38 (2013) 459.
[10] S. De Wolf, A. Descoeudres, Z.C. Holman, C. Ballif, Green 2 (2012) 7.
[11] S. Taira, Y. Yoshimine, T. Baba, M. Taguchi, H. Kanno, T. Kinoshita, H. Sakata, E. Maruyama, M. Tanaka, Proc. 22nd EU PVSEC, Milan, Italy (2007) 932.
[12] B. Bazer-Bachi, C. Oliver, B. Semmache, Y. Pellegrin, M. Gauthier, N. Le Quang, M. Lemiti, Proc. 26th EU PVSEC, Hamburg, Germany (2011) 1155.
[13] L.D. Bartholomew, N.M. Gralenski, J.C. Sisson, G.U. Pignatel, Eur. T. Telecommun. 1 (1990) 167.
[14] P. Rothhardt, C. Demberger, A. Wolf, D. Biro, En. Proc. 38 (2013) 305.
[15] B.J. Pawlak, T. Janssens, S. Singh, I. Kuzma-Filipek, J. Robbelein, N.E. Posthuma, J. Poortmans, F. Crisstiano, E.M. Bazizi, Prog. Photovoltaics. Res. Appl. 20 (1) (2012) 106.
[16] M.B. Spitzer, C.J. Keavney, Appl. Phys. Lett. 47 (7) (1985) 731.
[17] D.L. Meier, V. Chandrasekaran, H.P. Davis, A.M. Payne, X. Wang, V. Yelundur, J.E. O'Neill, Y.-W. Ok, F. Zimbardi, A. Rohatgi, IEEE Journ. Photovolt. 1 (2) (2011) 123.
[18] J. Armand, C. Oliver, B. Semmache, M. Gauthier, A. Foucaran, Y. Cuminal, Proc. 26th EU PVSEC, Hamburg, Germany (2011) 1309.
[19] H. Mehrer, Diffusion in Solids, Springer, Berlin, Heidelberg (2007).
[20] W. Kern, D. Puotinen, RCA Review 31 (1970) 187.
[21] D.E. Kane, R.M. Swanson, Proc. 18th IEEE PVSC, Las Vegas, USA (1985) 578.
[22] M.J. Kerr, A. Cuevas, J. Appl. Phys. 91 (4) (2002) 2473.
[23] J.H. Ranzmeyer, Y. Schiele, G. Hahn, B. Terheiden, to be published in Proc. 28th EU PVSEC, Paris, France (2013).